Short time transient thermal behavior of solid-state microrefrigerators

Y. Ezzahri, J. Christofferson, G. Zeng, A. Shakouri

Short time transient thermal behavior of solid-state microrefrigerators

Y. Ezzahri, J. Christofferson, G. Zeng, and A. Shakouri

Citation: Journal of Applied Physics **106**, 114503 (2009); doi: 10.1063/1.3266173
View online: http://dx.doi.org/10.1063/1.3266173
View Table of Contents: http://scitation.aip.org/content/aip/journal/jap/106/11?ver=pdfcov
Published by the AIP Publishing

Short time transient thermal behavior of solid-state microrefrigerators

Y. Ezzahri,[a] J. Christofferson, G. Zeng, and A. Shakouri[b]
Department of Electrical Engineering, University of California Santa Cruz, California 95064, USA

(Received 26 August 2009; accepted 27 October 2009; published online 8 December 2009)

We present detailed experimental and theoretical studies of the short time transient thermal behavior of SiGe superlattice microrefrigerators on a chip. Transient temperature profiles of microrefrigerator devices of different sizes are obtained using thermoreflectance technique. Thermal imaging with submicron spatial resolution, 0.1 K temperature resolution, and 100 ns temporal resolution is achieved. The dynamic behavior of the microrefrigerators shows an interplay between Peltier and Joule effects. Peltier cooling appears first with a time constant of about 10–30 μs, then Joule heating in the device starts taking over with a time constant of about 50–150 μs. The experimental results agree very well with the theoretical predictions based on thermal quadruple method. The difference in the two time constants can be explained considering the three-dimensional thermal resistances and capacitances of the microrefrigerator. In addition this shows that the Joule heating at the top metal/semiconductor interface does not dominate the microrefrigerator performance. Experimental results show that under high current pulsed operation, the microrefrigerator device can provide cooling for about 30 μs, even though steady state measurements show heating. © *2009 American Institute of Physics*. [doi:10.1063/1.3266173]

I. INTRODUCTION

Thermoelectric coolers are used for temperature stabilization and control of microelectronic and optoelectronic components. Excess heat generation and thermal management problems have grown with rapid development of very large scale integration technology, creating barriers to increase operation speeds and decrease feature sizes in optoelectronic and microelectronic applications. Conventional Bi_2Te_3 thermoelectric coolers have small cooling power densities and relatively slow transient response, on the order of 10–100 s.[1] Recently, thin film Bi_2Te_3 superlattice coolers have been demonstrated for hot spot removal on the back of the chip.[2] The cooling through a 700 μs thick silicon substrate will have a time response on the order of ~6 ms. On the other hand, Si/SiGe superlattice structures have demonstrated room temperature on chip cooling with cooling power densities exceeding 680 W/cm^2.[3] SiGe-based microrefrigerators are attractive for their potential monolithic integration with Si microelectronics. Because of the direct contact with the hot spot and film thicknesses in 3–5 μms range, they can have a much faster transient response, which is the basis of the current paper. Furthermore, combination of the solid-state cooling with other conventional cooling techniques such as liquid cooling[4] offers an additional degree of freedom both to control the overall temperature of the chip and to remove hot spots.[5]

Much work has been conducted in the past to study the cooling performance of three-dimensional (3D) SiGe-based microrefrigerators both theoretically and experimentally in steady state or direct current (dc) and alternative current (ac) regimes.[6–9] SiGe-based microrefrigerator cooling performance is based on the thermoelectric effect with thermionic enhancement.[10,11] Both superlattice based on Si/SiGe and also bulk SiGe thin film devices have been fabricated and characterized. Direct measurement of the cooling and cooling power density, along with material characterization, has allowed extracting the key factors limiting the performance of these microrefrigerators.[3] The transient thermal behavior is a third regime that is important not only for improving the microrefrigerator device performance but also for verifying thermal models. It is well known that bulk material BiTe thermoelectric devices can have a better cooling performance under pulsed mode operation,[12] meaning that they can momentarily reach a colder temperature than when measured in the steady state. A similar behavior was predicted for the 3D SiGe-based thin film microrefrigerator devices if the metal-semiconductor contact resistance does not dominate. However, limited metrology methods had prevented measurements.

In this paper, we present experimental and theoretical studies of the short time transient thermal behavior of 3D SiGe-based microrefrigerators. The theoretical modeling is based on using thermal quadruple method (TQM),[13] and measurements are performed using thermoreflectance (TR) thermal imaging technique.[14] Transient temperature profiles of 3D SiGe-based superlattice microrefrigerator devices of different sizes are obtained. The dynamic behavior of these microrefrigerators shows an interplay between Peltier and Joule effects. Experimental results show that under high current pulsed operation, the microrefrigerator device can provide cooling for about 10–30 μs, even though steady state measurements show heating.

Temperature distribution on the top metal lead connected to the microrefrigerator cold junction shows the interplay between Joule heating in the metal as well as heat conduction to the substrate. Modeling is used to study the effect of different physical and geometrical parameters of the device

[a]Electronic mail: younes@soe.ucsc.edu.
[b]Electronic mail: ali@soe.ucsc.edu.

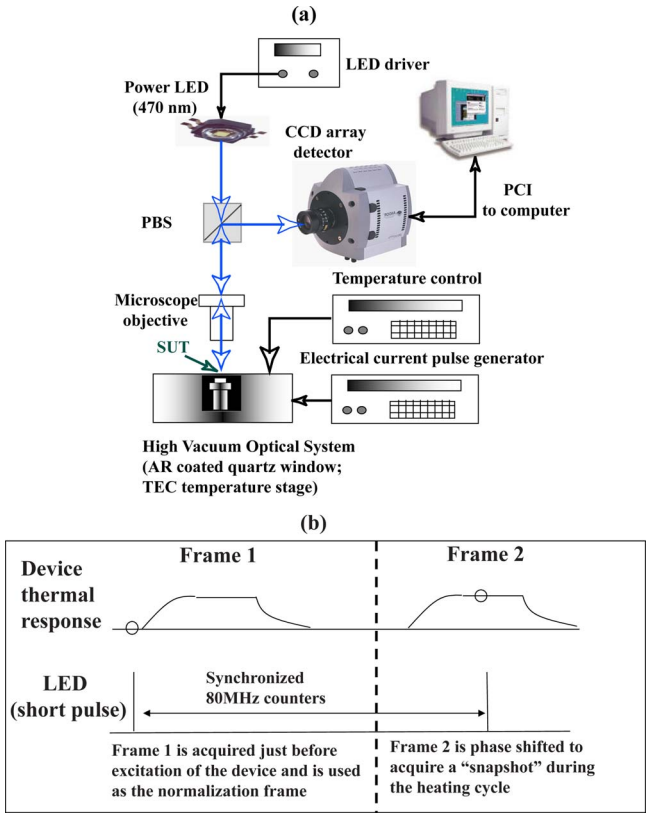

FIG. 1. (Color online) (a) Schematic of a typical TR imaging setup. (b) Transient thermal imaging scheme illustrating timing of a short pulse LED for acquisition of a thermal snapshot of the device during the temperature cycle. By utilizing separate phase locked, programmable counters, different phases of the temperature cycle can be obtained.

on its transient cooling. 3D geometry of heat and current flow in the device plays an important role. One of the goals is to maximize cooling over the shortest time scales.

II. TR THERMAL IMAGING SETUP AND SAMPLE DESCRIPTION

To investigate the transient thermal behavior of 3D SiGe thin film superlattice microrefrigerators, we have used TR imaging technique.[14] This is one of the most sensitive thermal measurement techniques and offers much higher spatial, thermal, and temporal resolutions than infrared (IR) imaging. It is an optical noncontact and nondestructive tool for device thermal characterization that is based on the very small (0.01%/K) temperature dependence of the material reflection coefficient.[14–16] It is an active technique that utilizes light of the visible spectrum, usually a blue (~450 nm) or green (~530 nm) light emitting diode (LED), but in general can be optimized to the surface material of the device under test.[14–16] Figure 1(a) shows a schematic of a typical TR imaging setup. For thermal transient measurements, TR is advantageous because it is an active technique. During the device heating cycle, very bright, short light pulses are reflected off the device, and the duration of the LED light pulse is what determines the temporal image resolution.

In TR imaging experiments, transient thermal information can be obtained using either time domain or frequency domain techniques.[15,16] The main challenge of such measurements is to resolve the small TR signal among the various noise sources, and so extensive image averaging and filtering are used. In our experiment, we have pursued a time domain, pulsed illumination technique, for several reasons, one primary reason being the simplicity in the setup and lack of complex computer computation on the high-resolution charge coupled device (CCD) data, allowing for more averaging per unit time. Additionally, visualization of the time domain transient response is sometimes more intuitive, and results can be analyzed using network identification by deconvolution method.[17] The latter is a powerful method to extract information about the various thermal resistances and capacitances of the device under study along the heat flux propagation path. Finally, by utilizing a high speed imaging laser diode that can be pulsed on the picosecond scale, the time domain transient TR technique has the potential to provide ultrashort time scale (approximately picoseconds) thermal images for characterization of material properties under excitation from a heating laser source. The transient TR experiment presented here utilizes a similar principle to the pump-probe transient TR experiment performed with a femtosecond laser.[18] The primary difference being that in the case of transient TR imaging, the heating is created electrically rather than optically. In this experiment, the present limit for short time scale thermal imaging is 100 ns, limited by the short pulse turn-on time of the LED used. At higher speeds, care must be taken to provide high-speed packaging for the LED, and additionally coaxial biasing probes must be used for device biasing.

Previous work on CCD based TR transient measurements[19] used a very simple single pulse "boxcar averaging technique," which is sufficient to find transient information to the microsecond scale; however, as the time resolution increases (shorter light pulses) there is less light available on the CCD and the temperature sensitivity is decreased. The solution allowing for 100 ns images, depicted in Fig. 1(b), is to provide many short light pulses for each CCD frame, and as long as we maintain precise timing (phase lock) between the device excitation pulse and the LED illumination pulse, it becomes possible to obtain a single thermal "snapshot" of the device heating at a precise time in the heating cycle. The system was implemented using a combination of National Instruments programmable counter/time boards and transistor transistor logic, necessary for the precise timing of signals. Because of the small TR coefficient κ, it becomes necessary to compare the value of the reflection coefficient at any time in the heating cycle to the value when the device is "off" R_0, which removes the large dc term. At any time of the heating cycle, the CCD frames are averaged and differenced to obtain the relative change in the reflection coefficient $(\Delta R/R_0)$, which is proportional to the change in the device surface temperature (ΔT) as a function of time $\Delta R/R_0(t)=\kappa\times\Delta T(t)$. More technical details on the experiment can be found in the recent work by Christofferson *et al.*[20]

Figure 2(a) shows an optical picture of SiGe-based microrefrigerators with three different sizes. Figure 2(b) illustrates the schematic cross sectional view of the 3D microrefrigerator that we consider in the theoretical modeling. The

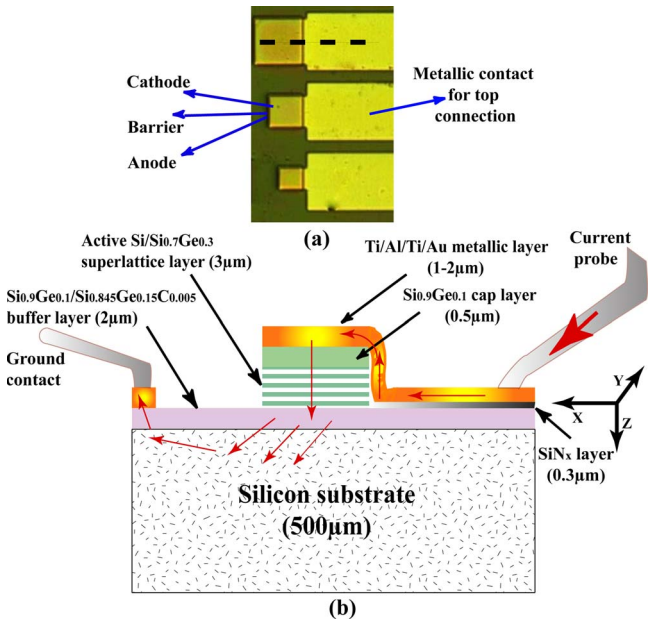

FIG. 2. (Color online) (a) Optical picture of three different 3D SiGe-based microrefrigerator device sizes. (b) Schematic of the microrefrigerator cross sectional view; the arrows indicate the direction of the electrical current.

microrefrigerator is composed of four layers: the main active layer is a 3 μm $Si/Si_{0.7}Ge_{0.3}$ superlattice with p-type doping concentration of 5×10^{19} cm^{-3}. The buffer layer is a 1 μm thick $Si_{0.9}Ge_{0.1}$ film followed by a 1 μm thick $Si_{0.9}Ge_{0.1}/Si_{0.845}Ge_{0.15}C_{0.005}$ superlattice with the same doping concentration as the active layer. The buffer layer is deposited on top of the Si substrate in order to reduce the lattice mismatch strain between the substrate and the superlattice.[21] On top of the superlattice layer, a 0.5 μm $Si_{0.9}Ge_{0.1}$ cap layer with higher doping concentration of 5×10^{20} cm^{-3} was included in order to improve the Ohmic contact between the metal and the semiconductor layer. A 0.3 μm SiN_x insulating layer is added underneath the top metal lead, to prevent any current leaking from the probe into the substrate; thus the current path is confined from the probe to the top of the active Si/SiGe superlattice layer before being distributed into the substrate. A 1–2 μm Ti/Al/Ti/Au layer was evaporated on top of the sample for electrical contact. A detailed description of the composition with growth parameters of the 3D SiGe-based microrefrigerator can be found in Ref. 22.

III. THERMOELECTRIC AND THERMIONIC COOLING

In a 3D SiGe-based microrefrigerator, the Peltier cooling occurs at the top metal layer/SiGe active layer junction and also at the buffer layer/substrate junction when the device is excited by an electrical current. The density of heat exchange at each junction is characterized by the effective Seebeck coefficient difference across the junction, and it is proportional to both current intensity and junction temperature.[1] Because of the difference in the Seebeck coefficient values at various interfaces, Peltier cooling or heating is created depending on the direction of the electrical current.[1]

In the case where the active layer is a superlattice structure, in addition to thermoelectric cooling, there is a thermionic cooling as it was shown by Shakouri *et al.*[10,11] and Mahan *et al.*,[23] which is an evaporative selective hot electron filtering effect.

Assuming small current densities, we can define an effective Seebeck coefficient for the solid-state thermionic cooling analogous to linear thermoelectric effects. The heating or cooling density at interfaces can then be considered as a linear function of the current intensity. In our model, we assume that the effective Seebeck coefficient takes into account both thermoelectric and thermionic phenomena.

IV. THEORETICAL MODEL AND SIMULATION

Our theoretical model is based on the TQM. TQM is a general analytical approach based on solving Fourier diffusive classical heat equation in Laplace domain by assuming a zero initial temperature. This method can be used to calculate electrical and thermal responses in a 3D geometry and in time-dependent or ac regimes, thus making it possible to distinguish, in some cases, the Peltier effect from the Joule effect. In the case of a pure sine wave electrical excitation, the Peltier effect appears at the same frequency as the operating current, whereas the Joule effect appears at the double frequency. The precision of the TQM allows its application in the detailed characterization of thermoelectric material properties.[24] This method has been used to model the behavior of a conventional thermoelectric couple (Bi_2Te_3),[24] and the dynamical behavior and the cut-off frequency of the 3D SiGe-based microrefrigerator.[8] Recently, we have also used the limit of the TQM at long times (i.e., steady state behavior) to model the cooling performance of the 3D SiGe-based microrefrigerators in the dc regime.[9] The results agree very well with thermocouple and TR measurements.[8,9] In the model presented herein this paper, thermophysical properties of the microrefrigerator are assumed to be temperature independent. In this model, the different thermal quantities of the microrefrigerator including the top surface temperature variation, and the cooling power density, are calculated by taking into account all possible mechanisms of heat generation and conduction within the entire device. 3D heat and current spreading in the substrate is taken into account using analytic formulas. Besides, heat generation and conduction in the top metal lead connected to the cold junction are also calculated via the TQM.

The thicknesses of the different layers, including the active Si/SiGe superlattice layer, are several orders of magnitude larger than the mean free path of both electrons and phonons.[25] Hence, we can assume a diffusive regime, and Fourier equation can be applied to describe heat transport inside the sample. The thickness of the whole structure is very small compared to that of the substrate; moreover, all Peltier sources are uniform on all junction plans; the heat transfer across the sample can be considered one-dimensional in the cross-plane direction of the device. We will assume the conditions to be adiabatic and neglect both the side and surface losses caused by convection radiation. This can be justified due to the small dimensions of the microrefrigerator and small cooling temperatures. Our device is formed of four essential layers.

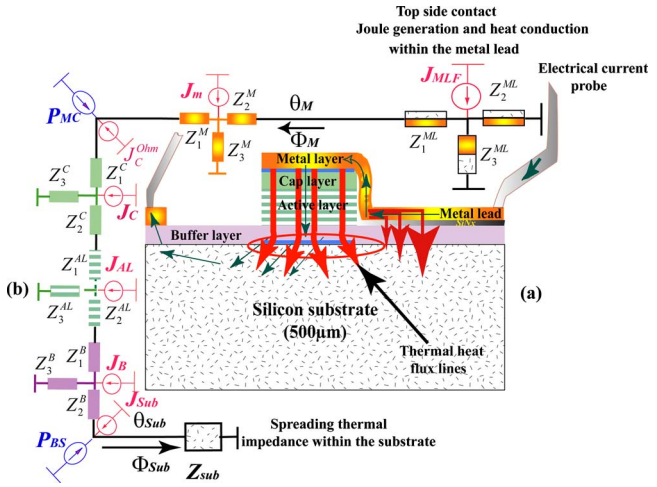

FIG. 3. (Color online) (a) Schematic of the microrefrigerator cross sectional view. (b) Thermal quadruple circuit associated with the heat transfer within the entire microrefrigerator operating either in the transient or ac regimes.

In a previous work, we presented a detailed description of the application of the TQM to model the cooling performance of 3D SiGe-based microrefrigerators in the dc regime.[9] In this section, we will give an overview of the TQM to model the short time transient thermal behavior of these microrefrigerators. In adiabatic conditions, the solution of the Fourier equation in Laplace domain for a passive, linear, isotropic, and homogeneous medium gives a linear relation between temperature-heat flux vectors at both ends of the medium. The transfer matrix of each layer i can be put in the form

$$\begin{pmatrix} \theta_i \\ \phi_i \end{pmatrix}_{\text{in}} = \begin{pmatrix} A_i & B_i \\ C_i & D_i \end{pmatrix} \begin{pmatrix} \theta_i \\ \phi_i \end{pmatrix}_{\text{out}} = \begin{pmatrix} ch(q_i e_i) & \frac{1}{K_i} sh(q_i e_i) \\ K_i sh(q_i e_i) & ch(q_i e_i) \end{pmatrix} \times \begin{pmatrix} \theta_i \\ \phi_i \end{pmatrix}_{\text{out}} = M_i \begin{pmatrix} \theta_i \\ \phi_i \end{pmatrix}_{\text{out}}, \tag{1}$$

where $q_i = \sqrt{p/\alpha_i}$, p is Laplace parameter, $K_i = \beta_i q_i \Sigma$, and $\alpha_i = \beta_i/(\rho C)_i$ is the thermal diffusivity of the layer i, and β_i, $(\rho C)_i$, e_i, and Σ are the thermal conductivity, specific heat per unit volume, thickness, and cross sectional area of the plan isothermal surface of the layer i, respectively.

The characteristics of this matrix, namely, $A=D$, and $\text{Det}(M)=1$, are typical for a transfer matrix of a symmetrical system. Such a system remains unchanged if one reverses the axis of propagation, and can be related to the properties of a passive four-terminal network, which can be represented by three impedances connected in a "T" shape circuit, as shown in Fig. 3(b). This figure represents the thermal quadruple system of the entire microrefrigerator device. We must note here that the ground level corresponds to room temperature, the impedances are thermal, and they are functions of the transfer matrix coefficients

$$Z_1^i = Z_2^i = \frac{A_i - 1}{C_i}, \quad Z_3^i = \frac{1}{C_i}. \tag{2}$$

This representation by impedances corresponds to the relation between boundary conditions.

To model the short time transient thermal behavior of the microrefrigerator, we suppose the device to be excited by a step-unit electrical current of amplitude I_0 as follows:

$$I_e(t) = I_0 \times H(t), \tag{3}$$

where $H(t)$ represents Heaviside function. In this case, the matrix relation between the temperature-heat flux vectors at the ends of each layer i becomes

$$\begin{pmatrix} \theta_i \\ \phi_i \end{pmatrix}_{\text{in}} = \begin{pmatrix} ch(q_i e_i) & \frac{1}{K_i} sh(q_i e_i) \\ K_i sh(q_i e_i) & ch(q_i e_i) \end{pmatrix} \begin{pmatrix} \theta_i \\ \phi_i \end{pmatrix}_{\text{out}} - \begin{pmatrix} Z_1^i Y_i \\ Y_i \end{pmatrix} = M_i \begin{pmatrix} \theta_i \\ \phi_i \end{pmatrix}_{\text{out}} - \begin{pmatrix} Z_1^i Y_i \\ Y_i \end{pmatrix}, \tag{4}$$

where Y_i represents the heat source inside each layer i. Y_i is given by

$$Y_i = \frac{R_i^{\text{ele}} I_0^2}{p} \times \frac{sh(q_i e_i)}{q_i e_i}, \tag{5}$$

where R_i^{ele} represents the electrical resistance of each layer i.

The application of Kirchhoff laws to the thermal quadruple system of Fig. 3(b) allows us to get a matrix relation between

$$\begin{pmatrix} \theta_{C_M} \\ \phi_{C_M} \end{pmatrix} \quad \text{and} \quad \begin{pmatrix} \theta_{C_{\text{sub}}} \\ \phi_{C_{\text{sub}}} \end{pmatrix},$$

the temperature-heat flux vectors at the top metal layer, and the interface buffer-layer/substrate, respectively. This matrix relation represents the heat transfer within the entire device in Laplace domain

$$\begin{pmatrix} \theta_{C_M} \\ \phi_{C_M} \end{pmatrix} = M_M M_{\text{CL}} M_{\text{AL}} M_{\text{BL}} \begin{pmatrix} \theta_{C_{\text{sub}}} \\ \phi_{C_{\text{sub}}} - P_{BS} \end{pmatrix} - M_M \begin{pmatrix} 0 \\ P_{MC} + Y_C^{\text{Ohm}} \end{pmatrix} - \begin{pmatrix} \Gamma \\ \Delta \end{pmatrix}. \tag{6}$$

The matrix M_i, $i=M,\text{CL},\text{AL},\text{BL}$, represents respectively, the heat transfer matrix of the metal layer, cap layer, active layer, and buffer layer, where

$$\begin{cases} P_{MC} = (S_M - S_{\text{AL}}) \dfrac{I_0 T_0}{p} \\ P_{BS} = (S_{\text{AL}} - S_{\text{sub}}) \dfrac{I_0 T_0}{p} \\ Y_C^{\text{Ohm}} = \dfrac{R_C^{\text{Ohm}} I_0^2}{p} \\ \Gamma = (Z_1^{\text{BL}} E + F) Y_{\text{BL}} + (Z_1^{\text{AL}} I + J) Y_{\text{AL}} + (Z_1^{\text{CL}} A_M + B_M) Y_{\text{CL}} + Z_1^M Y_M \\ \Delta = (Z_1^{\text{BL}} G + H) Y_{\text{BL}} + (Z_1^{\text{AL}} K + L) Y_{\text{AL}} + (Z_1^{\text{CL}} C_M + D_M) Y_{\text{CL}} + Y_M \end{cases} \tag{7}$$

with

$$\begin{cases} M_M M_{\mathrm{CL}} M_{\mathrm{AL}} M_{\mathrm{BL}} = \begin{pmatrix} A & B \\ C & D \end{pmatrix} \\ M_M M_{\mathrm{CL}} M_{\mathrm{AL}} = \begin{pmatrix} E & F \\ G & H \end{pmatrix} \\ M_M M_{\mathrm{CL}} = \begin{pmatrix} I & J \\ K & L \end{pmatrix}. \end{cases} \tag{8}$$

S_M, S_{AL}, and S_{sub} are the absolute Seebeck coefficients of the metal layer, active Si/SiGe superlattice layer, and substrate, respectively. The effective active layer Seebeck coefficient S_{AL} includes both thermoelectric and thermionic contributions. T_0 is the average temperature of the junction. For small excitation current amplitudes, previous simulations in the general ac case showed that linear approximation is still valid and approximating the interface temperature with room temperature is reasonably correct.[8,9,24] For this reason, in the whole simulation, we keep the average temperature of the junctions equal to the room temperature of 300 K.[8,9,24]

The relation between the heat flux at the interface top metal lead/microrefrigerator and the temperature variation at the top surface of the latter is given by[9]

$$\begin{cases} \phi_{C_M} = -\delta_{\mathrm{ml}} \tanh(q_{\mathrm{ml}} l_{\mathrm{ml}}) \theta_{C_M} + \dfrac{R_{\mathrm{ml}}^{\mathrm{ele}} I_e^2}{p} \gamma_{\mathrm{ml}} \tanh(q_{\mathrm{ml}} l_{\mathrm{ml}}) \\ \delta_{\mathrm{ml}} = \beta_M w_{\mathrm{ml}} e_M q_{\mathrm{ml}}, \quad \gamma_{\mathrm{ml}} = \dfrac{1}{q_{\mathrm{ml}} l_{\mathrm{ml}}} \\ q_{\mathrm{ml}}^2 = \dfrac{p}{\alpha_M} + \dfrac{H_{\mathrm{eff}}}{\beta_M e_M}, \end{cases} \tag{9}$$

where w_{ml} and l_{ml} are the width and the length of the top metal lead, respectively.[9] H_{eff} is an effective heat transfer coefficient that describes heat conduction from the bottom surface of the metal lead through the SiN_x layer and the buffer layer into the silicon substrate.[9,26] As for the microrefrigerator, the top metal lead surface is considered adiabatic. Due to the difficulty of solving analytically the two-dimensional dynamic heat spreading equation into the substrate, and in the sake of having a compact analytical model, we have assumed, as a first approximation, H_{eff} to be given by the same expression as in the steady state case.[9,26]

The substrate is thermally thick, and its 3D effect will be contained in what is called the *spreading thermal impedance* $Z_{\mathrm{sub}}^{\mathrm{th}}$. This impedance results from the spreading of heat flux lines when heat flows through the interface of two media of different geometries. In the approximation of cylindrical geometry for both the microrefrigerator and the substrate, the spreading thermal impedance for a uniform heat flux distribution on the contact disk $[0,r]$ is given by[13]

$$Z_{\mathrm{sub}}^{\mathrm{th}} = \frac{8}{3\pi^2 \beta_{\mathrm{sub}} r \left(1 + \dfrac{8r}{3\pi} \sqrt{\dfrac{p}{\alpha_{\mathrm{sub}}}}\right)}, \tag{10}$$

where $r = \sqrt{\Sigma/\pi}$ is the radius of the contact disk between the two media, and β_{sub} and α_{sub} are the thermal conductivity and diffusivity of the substrate, respectively.

In addition to the thermal spreading inside the substrate, there is also an electrical current spreading. Joule heating is mainly localized at the interface buffer layer/substrate.[27] This electrical spreading is characterized by a spreading of the electrical current density lines in the substrate. Heat current flow could be different from electrical current flow due essentially to the notion of skin effect related to the electrical current in the very high frequency ac regime. In the transient regime at the time scale of 100 ns, skin effect could be neglected. In fact, using the properties of the silicon substrate we can easily show that the skin depth varies from 90 000 to 900 μm for an excitation frequency from 1 kHz to 10 MHz. These values are still very large compared to the size of the microrefrigerator. Electrical spreading within the substrate can be characterized by a spreading electrical resistance calculated by analogy to the spreading thermal resistance in the dc regime[9]

$$R_{\mathrm{sub}}^{\mathrm{ele}} = \frac{8}{3\pi^2 \sigma_{\mathrm{sub}} r}, \tag{11}$$

where $r = \sqrt{\Sigma/\pi}$ is the radius of the contact disk between the microrefrigerator and the substrate, and σ_{sub} is the electrical conductivity of the substrate.

The relation between the heat flux at the interface buffer layer/substrate and the temperature at this interface is given by the expression

$$\begin{cases} \phi_{C_{\mathrm{sub}}} = \dfrac{\theta_{C_{\mathrm{sub}}}}{Z_{\mathrm{sub}}^{\mathrm{th}}} - \dfrac{1}{2} Y_{\mathrm{sub}} \\ Y_{\mathrm{sub}} = \dfrac{R_{\mathrm{sub}}^{\mathrm{ele}} I_e^2}{p}. \end{cases} \tag{12}$$

The final expression of the microrefrigerator top surface temperature in Laplace domain is obtained by combining Eqs. (6)–(9) with Eq. (12) as follows:

$$\begin{cases} \theta_{C_M} = \dfrac{1}{\chi^{\mathrm{tot}}} \left\{ (AD - BC) \left(P_{BS} + \dfrac{1}{2} Y_{\mathrm{sub}} \right) + \left[(AD_M - B_M C) + \dfrac{BD_M - B_M D}{Z_{\mathrm{sub}}^{\mathrm{th}}} \right] (P_{MC} + Y_C^{\mathrm{Ohm}}) + \left(A + \dfrac{B}{Z_{\mathrm{sub}}^{\mathrm{th}}} \right) \left[\Delta + \dfrac{R_{\mathrm{ml}}^{\mathrm{ele}} I_e^2}{p} \gamma_{\mathrm{ml}} \tanh(q_{\mathrm{ml}} l_{\mathrm{ml}}) \right] - \left(C + \dfrac{D}{Z_{\mathrm{sub}}^{\mathrm{th}}} \right) \Gamma \right\} \\ \chi^{\mathrm{tot}} = \delta_{\mathrm{ml}} \tanh(q_{\mathrm{ml}} l_{\mathrm{ml}}) \left(A + \dfrac{B}{Z_{\mathrm{sub}}^{\mathrm{th}}} \right) + C + \dfrac{D}{Z_{\mathrm{sub}}^{\mathrm{th}}}. \end{cases} \tag{13}$$

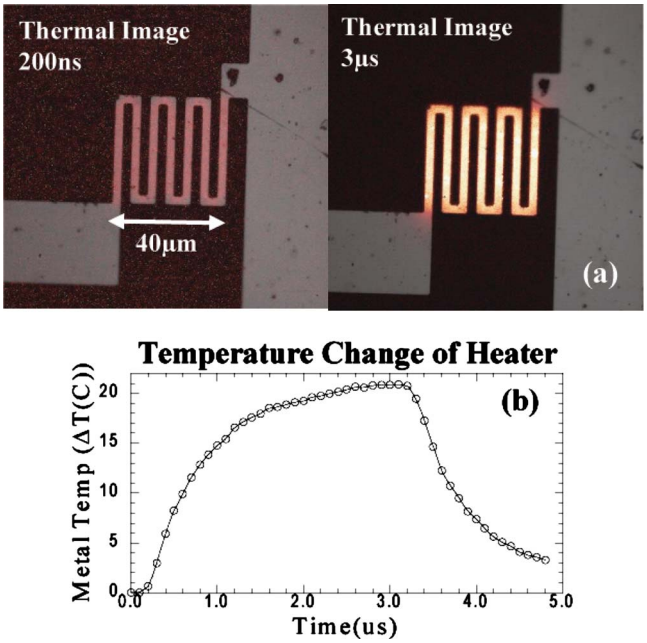

FIG. 4. (Color online) (a) Transient thermal images of a 40×40 μm^2 metal heater fabricated on a silicon substrate. (b) Thermal time response of the metal heater; data are taken from the thermal images in (a). The graph is generated by averaging ~80 pixels in the center of the heater for every 100 ns thermal image.

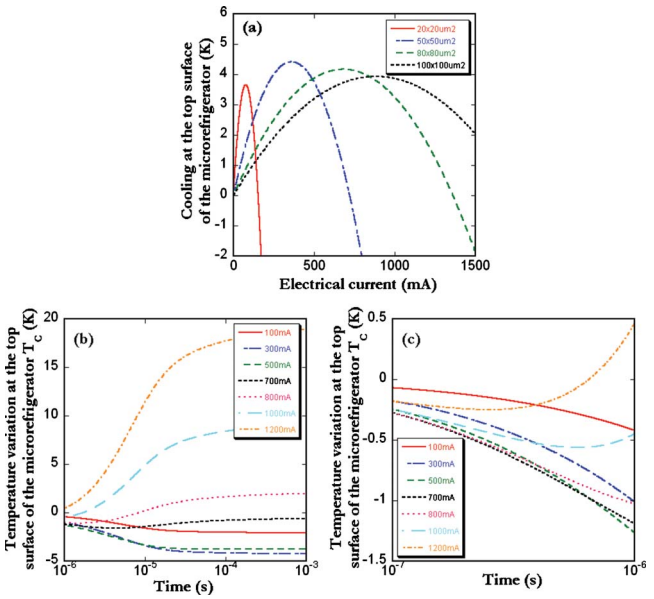

FIG. 5. (Color online) (a) Simulation of the steady state cooling for different microrefrigerator device sizes as a function of the applied electrical current. [(b) and (c)] Simulation of the transient temperature variation at the top surface of a 50×50 μm^2 microrefrigerator for different electrical current amplitudes over two different time intervals.

χ^{tot} describes the total thermal admittance seen by the microrefrigerator top surface.

The cooling power density at the microrefrigerator top surface is calculated by following a similar procedure as for the temperature, and the final expression in Laplace domain is given by

$$Q_{C_M} = \frac{1}{A + \frac{B}{Z_{sub}^{th}}}\left\{(BC - AD)\left(P_{BS} + \frac{1}{2}Y_{sub}\right) + \left[(B_M C - AD_M) + \frac{B_M D - BD_M}{Z_{sub}^{th}}\right](P_{MC} + Y_C^{Ohm}) + \left(C + \frac{D}{Z_{sub}^{th}}\right)\Gamma - \left(A + \frac{B}{Z_{sub}^{th}}\right)\left[\Delta + \frac{R_{ml}^{ele} I_e^2}{p}\gamma_{ml}\tanh(q_{ml} l_{ml})\right]\right\}. \quad (14)$$

The transformation to the time domain is performed using a numerical Laplace inverse transform algorithm such as Gaver–Stehfest's algorithm.[13]

V. RESULTS AND DISCUSSION

We start this section by discussing the transient thermal behavior of a simple device: a metal heater deposited on a silicon substrate. Figure 4(a) shows thermal images of a 40×40 μm^2 metal heater fabricated on a silicon substrate when excited with a 200mA, 3 μs pulse width with 25 ns rise time. The thermal images presented are a representation of the thermal data combined with the optical image in order to visualize the location of the heating compared to the device metal. The images, acquired at 200 ns, and 3 μs after excitation, show the fast response of the metal heater, and also that after 3 μs the heating begins to spread out to the contact layer. In Fig. 4(b), we report the transient thermal response of the heater obtained by choosing a region of the device metal and analyzing the thermal image series. The device has about 2 μs thermal response time, which is reasonable for a small metal heater fabricated on a silicon substrate. The images are taken every 100 ns and the rise and fall of the thermal transient is clearly seen. The data acquired were 50 images, averaged at 2 min each. There are a few factors that influence the overall thermal sensitivity of TR imaging, but probably the most important are the material dependent value of the TR coefficient κ, the sensitivity of the imaging sensor used, and the averaging time.[20]

To explore the short time transient thermal behavior of 3D SiGe-based microrefrigerators, two device sizes 50×50 and 80×80 μm^2 were thermally imaged and compared to theoretical predictions.

Let us first start with the theoretical predictions. The calculated steady state cooling of the 3D SiGe-based microrefrigerator is shown in Fig. 5(a) for four different device sizes as a function of the amplitude of the electrical current. The simulation shows that for each size, the device has an optimum current amplitude for which maximum cooling occurs. This optimum current value increases with the size of the device. For electrical current amplitudes lower than the optimum, linear Peltier cooling dominates, and for electrical current amplitudes higher than the optimum, quadratic Joule heating takes over. The Ohmic contact resistance at the top metal/semiconductor surface was taken to be $r_{oc} = 10^{-6}$ Ω cm^2, which is a realistic value for these devices.[3] Table I summarizes the thermophysical properties of the different layers in the microrefrigerator used in the simulations. The transient thermal behavior of a 50×50 μm^2 device is

TABLE I. Thermophysical properties of the different layers in the 3D SiGe-based microrefrigerator used in the TQM simulations.

Layer	Thickness (μm)	Density ρ(kg/m^3)	Heat capacity, C (J/kg K)	Seebeck coefficient (μV/K)	Electrical conductivity (Ω cm)$^{-1}$	Thermal conductivity (W m^{-1} K^{-1})
Metal	1	19 300	128	8	$150/T_0/L$ [a]	150
Cap	0.5	2 673	614	235	2884	9.6
Active Si/SiGe superlattice	3	2 663	632	235	365	8
Buffer	2	2 673	614	235	721	6.1
Substrate	Thermally thick	2 329	700	445	310	130

[a] T_0 represents the ambient temperature taken to be room temperature 300 K, and L is Lorentz number $L \approx 2.44 \times 10^{-8}$ V^2/K^2.

reported in Figs. 5(b) and 5(c) over two different time ranges. These figures show the simulation result of the temperature variation at the top surface of the microrefrigerator device as a function of time, as a response to a step electrical current pulse of different amplitudes. As we can see in this figure, for current amplitudes below the optimum value [Fig. 5(a)], the temperature decreases as a function of time to stabilize in the cooling regime. On the other hand, when the current amplitude is higher than the optimum value, the temperature first decreases to reach a minimum and then it starts increasing. More interestingly is that under high biasing current, the thin film device can momentary cool below the ambient [Figs. 5(b) and 5(c)], even though the steady state shows heating [Fig. 5(a)].

In Fig. 6(a), TR imaging results demonstrate clearly that we can capture the transient evolution of the microrefrigerator top surface temperature as it goes from cooling to heating. The thermal images are taken on the top surface of an 80×80 μm^2 Si/SiGe superlattice device and are acquired at 10, 20, and 50 μs. The frames are acquired every 10 μs and the images are the response to a 1.7 A, 166 μs electrical excitation pulse. The LED used has a duty cycle of 1%–2%.[20] These results confirm the simulation predictions in Fig. 5(b). Besides, from each thermal image, it is possible to obtain useful information about temperature distribution in the device and the sources of Peltier cooling and Joule heating. Figure 6(a) shows the thermal images, Fig. 6(b) displays the temperature transient in the center of the device, and Fig. 6(c) gives the temperature cross sections at different times. These data can be used to verify the details of the thermal models.[20]

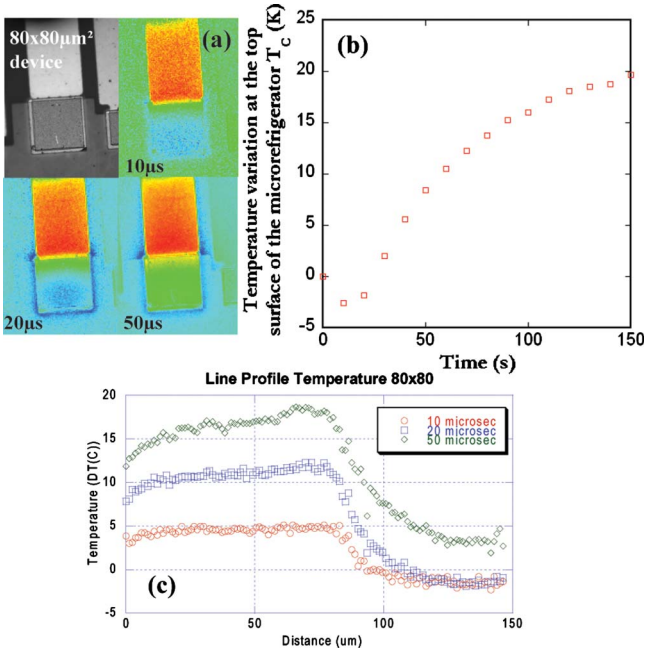

FIG. 6. (Color online) (a) Transient thermal images of an 80×80 μm^2 microrefrigerator in response to a 1.7 A, 166 μs pulse taken at 10, 20, and 50 μs. (b) Thermal transient response of the center region of the same microrefrigerator device. (c) Line profile along the dotted line in (a) from the contact layer across the device top surface at different time steps 10, 20, and 50 μs. At later times, the cooling is pushed to the far end of the device.

Figure 7 shows the experimental transient TR signal acquired from 500 ns to 500 μs on the top surface of a 50×50 μm^2 Si/SiGe-based superlattice microrefrigerator under 1 A current excitation. This is plotted in a logarithmic scale and compared with the TQM simulation. There is a reasonably good agreement between theory and experiment over three orders of magnitude in time scale. The dynamic behavior shows an interplay between Peltier and Joule effects. Peltier cooling is an interface effect located closer to the top surface of the device. It appears first with a time constant of about <10 μs. On the other hand, Joule heating is a volume or bulk effect that takes certain time to reach the surface. Joule heating in the device starts taking over with a time constant of about 50–150 μs. The difference in the two time constants can be explained considering the thermal resistances and capacitances of the microrefrigerator. In addition this shows that the Joule heating at the top metal/semiconductor interface does not dominate the

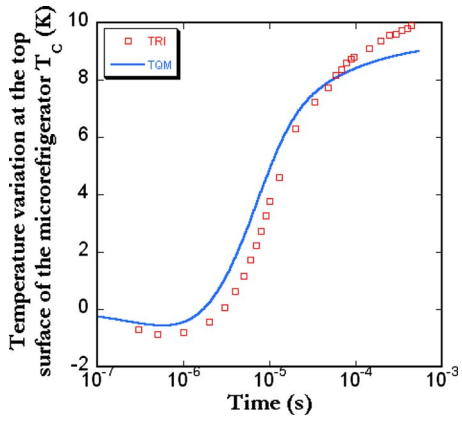

FIG. 7. (Color online) Comparison between the experimental TR imaging result and the TQM simulation of the temperature variation at the top surface of a 50×50 μm^2 microrefrigerator device under 1 A current excitation from 300 ns to 500 μs.

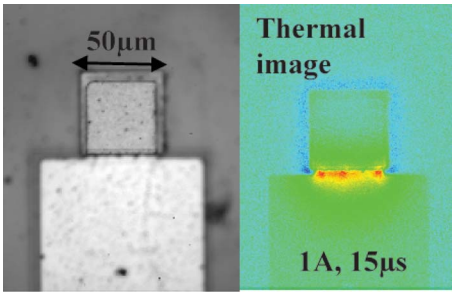

FIG. 8. (Color online) Optical and thermal images of a 50×50 μm^2 microrefrigerator device acquired at 15 μs after excitation. The device shows excessive heating at the junction between the device and the contact layer due to the poor metal coverage at the mesa side wall.

microrefrigerator performance. If this was the case, we would have obtained the same time constants for Peltier and Joule effects.

There are many material parameters that can be adjusted in the TQM simulations. One effect not included in the simulation is that of electrical current constriction/spreading, which occurs when the microrefrigerator device and the top metal lead have different widths. While a wider contact layer has less resistance, the constriction of current as the electrons move from a wide to a narrow region creates extra heating near the device. Since the heating in the contact layer is a surface effect, it would occur rapidly, with the same time response as the cooling effect, and it could limit the transient cooling. Figure 8 shows the thermal image of another 50×50 μm^2 microrefrigerator device under 1 A current excitation, 15 μs into the thermal cycle. Clearly seen in the thermal image is the excessive heating between the contact layer and the device surface, which is a nonideal effect resulting from imperfect metal coverage at the mesa.

Modeling is used to study the effect of different physical and geometrical parameters of the device on its transient cooling. We have already addressed the question of changing the physical properties,[28] and we focus here on the effect of geometrical properties, namely, the size of the microrefrigerator and the thickness of the active Si/SiGe superlattice layer. Figure 9(a) shows the calculated transient cooling of a 50×50 μm^2 device from 1 μs to 1 s as a response to a step electrical current. The results are shown for different thicknesses of the active Si/SiGe layer t_{AL}. For this simulation, r_{oc} is taken to be $r_{oc}=10^{-6}$ Ω cm^2 the same as before. The amplitude of the electrical current is chosen to be the one for which the temperature at the top surface of the device vanishes at the steady state. We can see how changing t_{AL} affects the maximum cooling and the shape of the transient temperature over the time interval. This behavior is well captured in the inset of Fig. 9(a) that shows the variation of the minimum transient temperature or maximum transient cooling as a function of t_{AL} for various device sizes. Different behaviors occur depending on the microrefrigerator size. This effect is due to the 3D geometry of heat and current flow in the device substrate. The maximum cooling has a slight minimum that is more pronounced for small sizes and disappears as the microrefrigerator size increases. Generally the maximum transient cooling increases by increasing t_{AL}. This behavior

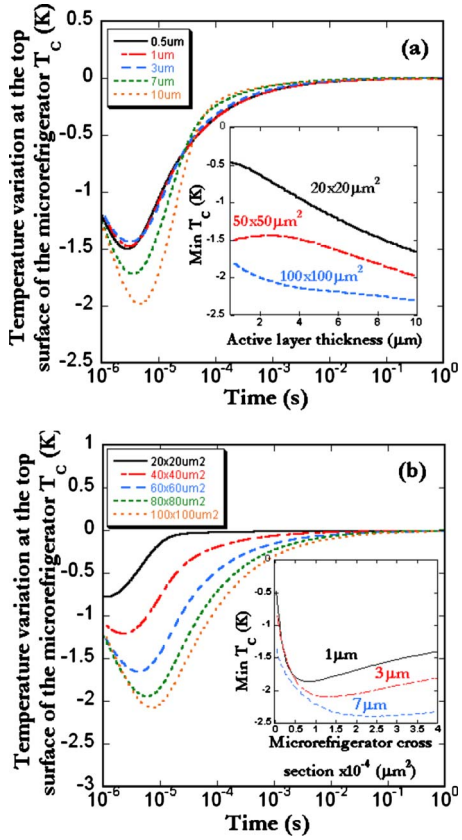

FIG. 9. (Color online) (a) Transient temperature variation as a function of time at the top surface of a 50×50 μm^2 microrefrigerator for different Si/SiGe superlattice active layer thicknesses t_{AL}. The inset shows the variation of minimum (T_C) as a function of t_{AL} for different microrefrigerator sizes. (b) Transient temperature variation as a function of time for different microrefrigerator device sizes with the same 3 μm Si/SiGe superlattice active layer thickness t_{AL}. The inset shows the variation of minimum (T_C) as a function of the microrefrigerator size for different thicknesses t_{AL}.

can be explained by considering the thermal capacitance of the active layer. The thermal capacitance increases by increasing t_{AL} and then it takes more time for Joule effect, which is a volume effect, to reach the top surface of the device where the temperature variation is considered. Since Peltier effect location does not change, this effect becomes more and more dominant as we increase t_{AL}.

Considering the same simulation conditions, Fig. 9(b) shows the transient cooling of different microrefrigerator sizes with the same 3 μm thick active Si/SiGe superlattice layer over the same time interval. The area between the horizontal axis and the curve increases with the device size. This means that larger microrefrigerator device sizes can maintain a considerable cooling performance that can go up to hundreds of milliseconds even though the steady state shows a zero temperature variation. We can also see in the inset of this figure that for a given thickness of the active layer, the maximum cooling at the top surface of the microrefrigerator exhibits an optimum device size that increases with the thickness of the active layer. This effect is again a consequence of the 3D geometry of heat and current flow in the device substrate.

As simplified as they are, the analytical solutions provided by the TQM reproduce very fairly the experimental

results of the transient thermal behavior of the 3D SiGe-based microrefrigerator. These solutions can be used as a guide to determine the key parameters and improve the transient cooling performance of the device.

VI. CONCLUSION

A CCD based TR thermal imaging system with 100 ns temporal, 200 nm spatial, and 0.1 K thermal resolutions has been used to acquire transient thermal images of microrefrigerators over four orders of magnitude in time, from 100 ns to 1 ms. The measured results on a 3D SiGe-based microrefrigerator device are in a reasonably good agreement with the TQM simulation. Simulation and experiment show that the device can achieve a cooling below ambient temperatures under moderate currents for the first few tens of microseconds, even though steady state shows a net heating. Depending on the microrefrigerator device size, this dynamic behavior shows an interplay between Peltier and Joule effects. Peltier cooling is an interface effect located closer to the top surface of the device. It appears first with a time constant of about 10–30 μs. On the other hand Joule heating is a volume or bulk effect that takes certain time to reach the surface. Joule heating in the device starts taking over with a time constant of about 50–150 μs. The difference in the two time constants can be explained considering the thermal resistances and capacitances of the microrefrigerator. Modeling is used to study the effect of different geometrical parameters of the device on its transient cooling. One of the goals is to maximize cooling over the shortest time scales.

ACKNOWLEDGMENTS

The authors would like to knowledge the support of the Interconnect Focus Center, one of the five research centers funded under the Focus Center Research Program, a DARPA and Semiconductor Research Corporation Program (Grant No. 59771-444040).

[1]D. M. Rowe, *Handbook of Thermoelectrics* (CRC, Boca Raton, FL, 1995).
[2]I. Chowdhury, R. Prasher, K. Lofgreen, G. Chrysler, S. Narasimhan, R. Mahajan, D. Koester, R. Alley, and R. Venkatasubramanian, Nat. Nanotechnol. **4**, 235 (2008).
[3]A. Shakouri, Proc. IEEE **94**, 1613 (2006).
[4]A. Bar-Cohen, M. Arik, and M. Ohadi, Proc. IEEE **94**, 1549 (2006).
[5]Y. Ezzahri and A. Shakouri, Proceedings of the Thermal Issues in Emerging Technologies (ThETA) II Conference, Cairo, Egypt, 17–20 December 2008 (unpublished).
[6]C. LaBounty, A. Shakouri, and J. E. Bowers, J. Appl. Phys. **89**, 4059 (2001).
[7]D. Vashaee, J. Christofferson, Y. Zhang, A. Shakouri, G. Zeng, C. LaBounty, X. Fan, J. Piprek, J. E. Bowers, and E. Croke, Microscale Thermophys. Eng. **9**, 99 (2005).
[8]Y. Ezzahri, S. Dilhaire, L. D. Patiño-Lopez, S. Grauby, W. Claeys, Z. Bian, Y. Zhang, and A. Shakouri, Superlattices Microstruct. **41**, 7 (2007).
[9]Y. Ezzahri, G. Zeng, K. Fukutani, Z. Bian, and A. Shakouri, Microelectron. J. **39**, 981 (2008).
[10]A. Shakouri and J. E. Bowers, Appl. Phys. Lett. **71**, 1234 (1997).
[11]A. Shakouri, E. Y. Lee, D. L. Smith, V. Narayanamurti, and J. E. Bowers, Microscale Thermophys. Eng. **2**, 37 (1998).
[12]Q. Zhou, Z. Bian, and A. Shakouri, J. Phys. D: Appl. Phys. **40**, 4376 (2007).
[13]D. Maillet, S. André, J. C. Batsale, A. Degiovanni, and C. Moyne, *Thermal Quadruples: Solving the Heat Equation Through Integral Transforms* (Wiley, Chichester, 2000).
[14]J. Christofferson and A. Shakouri, Rev. Sci. Instrum. **76**, 024903 (2005).
[15]S. Grauby, S. Dilhaire, S. Jorez, and W. Claeys, Rev. Sci. Instrum. **74**, 645 (2003).
[16]P. L. Komarov, M. G. Burzo, and P. E. Raad, Proceedings of the THERMINIC 12, Nice, Côte d'Azur, France, 27–29 September 2006 (unpublished).
[17]V. Székely and T. V. Bien, Solid-State Electron. **31**, 1363 (1988).
[18]Y. Ezzahri, S. Grauby, S. Dilhaire, J. M. Rampnoux, and W. Claeys, J. Appl. Phys. **101**, 013705 (2007).
[19]K. Maize, J. Christofferson, and A. Shakouri, Proceedings of the SEMITHERM 24, San Jose, CA, 16–20 March 2008 (unpublished).
[20]J. Christofferson, Y. Ezzahri, K. Maize, and A. Shakouri, Proceedings of the SEMITHERM 25, San Jose, CA, 15–19 March 2009 (unpublished).
[21]D. J. Paul, Semicond. Sci. Technol. **19**, R75 (2004).
[22]Y. Zhang, D. Vashaee, J. Christofferson, G. Zeng, C. LaBounty, J. Piprek, E. T. Croke, and A. Shakouri, Proceedings of the International Mechanical Engineering Congress and Exposition, Washington, DC, 16–21 November 2003 (unpublished).
[23]G. D. Mahan, J. O. Sofo, and M. Bartkowiak, J. Appl. Phys. **83**, 4683 (1998).
[24]L. D. Patino-Lopez, S. Grauby, Y. Ezzahri, W. Cleays, and S. Dilhaire, Proceedings of the 25th International Conference on Thermoelectrics, Vienna, Austria, 6–10 August 2006 (unpublished).
[25]J. M. Ziman, *Electrons and Phonons* (Oxford University Press, Oxford, 1960).
[26]P. Wang, A. B. Cohen, B. Yang, G. L. Solbrekken, and A. Shakouri, J. Appl. Phys. **100**, 014501 (2006).
[27]S. Dilhaire, Y. Ezzahri, S. Grauby, W. Cleays, J. Christofferson, Y. Zhang, and A. Shakouri, Proceedings of the 22nd International Conference on Thermoelectrics, La Grande Motte, France, 17–21 August 2003 (unpublished).
[28]Y. Ezzahri, J. Christofferson, K. Maize, and A. Shakouri, Proceedings of the MRS Spring Meeting, San Francisco, CA, 13–17 April 2009 (unpublished).